Nanoscale

ROYAL SOCIETY OF CHEMISTRY

COMMUNICATION

View Article Online
View Journal | View Issue

Cite this: *Nanoscale*, 2024, **16**, 11538

Received 25th March 2024,
Accepted 28th May 2024

DOI: 10.1039/d4nr01314j

rsc.li/nanoscale

Published on 30 May 2024. Downloaded on 5/21/2026 4:37:46 PM.

Near-infrared AIEgens for sulfatase imaging in breast cancer *in vivo*†

Lingling Xu,[a] Yu Deng,[a] Hang Gao,[b] Yuchen Yao,[a] Xiaoyang Liu,[a] Wenjun Zhan,[a] Gaolin Liang*[a,c] and Xianbao Sun *[a]

Aggregation-induced emission luminogens (AIEgens) enable highly sensitive and *in situ* visualization of sulfatase to benefit the early diagnosis of breast cancer (BC), but current sulfatase AIEgens always emit visible light (<650 nm). Herein, a near-infrared (NIR) AIEgen QMT-SFA is developed for sulfatase imaging *in vivo*. Hydrophilic QMT-SFA is cleaved by sulfatase to yield hydrophobic QMT-OH, which subsequently aggregates into nanoparticles to turn the AIE fluorescence "on", enabling sensitive sulfatase imaging in 4T1 cells and mouse models.

Breast cancer (BC) is the most frequently diagnosed malignant tumor in women worldwide, with high morbidity and mortality rates.[1,2] In clinical practice, mammography plays an essential role in BC screening, but it has limitations in the early diagnosis of BC due to its low sensitivity;[3] tissue biopsy can help diagnose BC but is commonly used until late cancer stages.[4] Therefore, it is of clinical importance to establish advanced methodologies for the early diagnosis of BC. To this end, some molecular or nanoprobes have been recently developed for sensitive and *in situ* detection of BC biomarkers (*e.g.*, matrix metalloproteinase, cathepsin, and sulfatase) at the molecular level, which benefits the identification of BC at early stages.[5] Among these biomarkers, sulfatase is a highly conserved sulfate-hydrolyzing protease which is overexpressed upon the occurrence of BC.[6,7] Thereby, sensitive imaging probes of sulfatase are highly desired for the early diagnosis of BC.

Among the various imaging modalities, fluorescence imaging shows unique advantages in biomarker detection, such as non-invasiveness and superior temporal and spatial resolution.[8–11] In recent years, a range of fluorescence probes have been devised for the sensitive imaging of sulfatase activity.[12] Of note, these fluorescence probes with aggregation-induced emission (AIE) characteristics (*i.e.*, AIEgens) have attracted high interest due to their small autofluorescence interference, low toxicity, and strong resistance to photobleaching.[13–16] However, current sulfatase AIEgens always emit visible light (<650 nm), which gives rise to non-negligible autofluorescence interference and inferior tissue penetration, thus severely hindering their further biological application and clinical translation.[17] In this regard, an AIEgen with a near-infrared (NIR) emission, which affords a higher signal-to-background ratio and deeper tissue penetration,[18,19] would benefit the sensitive imaging of sulfatase *in vivo*. However, so far, as we know, such sulfatase-activated AIEgens with NIR fluorescence emissions have not been reported.

Herein, a sulfatase-activatable NIR fluorescence probe (**QMT-SFA**) was fabricated, which contains an AIE luminophore (QMT)[13] and a hydrophilic sulfatase-cleavable sulfate moiety (Fig. 1). As we hypothesized, **QMT-SFA** exhibited an initially weak fluorescence emission under physiological conditions because the hydrophilic **QMT-SFA** molecules were dispersive. When the sulfate group in **QMT-SFA** was cleaved by sulfatase inside BC cells, the obtained hydrophobic **QMT-OH** aggregated into nanoparticles, which emitted bright NIR fluorescence through the AIE mechanism. In this study, **QMT-SFA** has been successfully applied to visualize sulfatase activity *in vivo*.

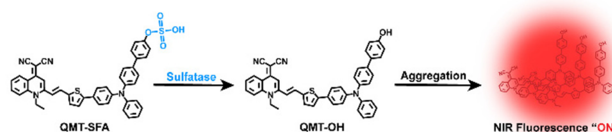

Fig. 1 Schematic illustration of the sulfatase-activatable near-infrared (NIR) aggregation-induced emission probe QMT-SFA.

[a]*State Key Laboratory of Digital Medical Engineering, School of Biological Science and Medical Engineering, Southeast University, Nanjing, Jiangsu 210096, China. E-mail: gliang@seu.edu.cn, xbsun@seu.edu.cn*
[b]*State Key Laboratory of Analytical Chemistry for Life Science, School of Chemistry and Chemical Engineering, Nanjing University, Nanjing, Jiangsu 210023, China*
[c]*Handan Norman Technology Co., Ltd, Guantao 057750, China*

† Electronic supplementary information (ESI) available. See DOI: https://doi.org/10.1039/d4nr01314j

 This journal is © The Royal Society of Chemistry 2024

Published on 30 May 2024. Downloaded on 5/21/2026 4:37:46 PM.

First, **QMT-SFA** was synthesized according to the procedure illustrated in Scheme S1,† and characterized by electrospray ionization mass spectrometry (ESI-MS, Fig. S1†). After synthesis, we initially explored the responsiveness of **QMT-SFA** toward sulfatase in phosphate buffered saline (PBS, 100 mM, pH 7.4, 1% DMSO). Briefly, **QMT-SFA** (10 μM) was incubated with 40 U mL^{-1} sulfatase at 37 °C for 1 h. The chemical evolution of **QMT-SFA** in response to sulfatase was traced by high-performance liquid chromatography (HPLC). As shown in Fig. 2a, 70% **QMT-SFA** (retention time: 11.6 min) was cleaved by sulfatase and converted to a new product, which shared the same retention time (18.0 min) as **QMT-OH**. ESI-MS results further certified that this compound (at 18.0 min) was **QMT-OH** (Fig. S2†). These results confirmed that **QMT-SFA** was successfully hydrolyzed by sulfatase to **QMT-OH**. Furthermore, molecular **QMT-SFA** could form into nanoparticles with an average diameter of ∼25.5 nm (Fig. 2b, S3 and S4†). We further recorded the fluorescence spectra to verify whether this sulfatase-triggered nanoparticle formation could turn the NIR AIE fluorescence "on". As shown in Fig. 2c, under the above conditions, **QMT-SFA** exhibited a low fluorescence signal at 660 nm, whereas the signals increased with the concentration (0–40 U mL^{-1}) of sulfatase, indicating that **QMT-SFA** was successfully activated by sulfatase to emit AIE fluorescence (Fig. 2c). Moreover, there was a linear relationship ($y = 0.04x + 0.12$, $R^2 = 0.97$) between the fluorescence intensity and the concentration of sulfatase within the range of 0–20 U mL^{-1} (Fig. 2d). The limit of detection (LOD) was calculated to be about 0.26 U mL^{-1}. These results indicated that **QMT-SFA** could be used as a sensitive probe for sulfatase detection *in vitro*.

Fig. 2 (a) HPLC analyses of 10 μM **QMT-SFA** (black) and 10 μM **QMT-SFA** treated with 40 U mL^{-1} sulfatase for 1 h (red), and 10 μM **QMT-OH** (blue). (b) TEM image of 10 μM **QMT-SFA** treated with 40 U mL^{-1} sulfatase. (c) Fluorescence response of **QMT-SFA** (10 μM) toward different levels of sulfatase. (d) The fitted relationship between the fluorescence intensity of **QMT-SFA** and sulfatase concentration. (e) Ribbon diagram of the binding interface between **QMT-SFA** and sulfatase. (f) 2D diagram of the interaction interface between **QMT-SFA** and sulfatase.

Molecular docking calculations were performed to study the binding affinity between **QMT-SFA** and sulfatase. The protein structure of sulfatase (PDB ID: 1AUK) was chosen for docking analysis.[6,17] As shown in Fig. 2e and f, **QMT-SFA** forms strong hydrophobic interactions with seven amino acids (Val91, Tyr379, His405, Ala478, Pro8, Val93 and Val477) and hydrogen bonds with five amino acids (Glu481, Gly402, Val91, Tyr379 and Ser403) of sulfatase. Meanwhile, there is also a Coulomb interaction between GLU481 of sulfatase and **QMT-SFA** (Table S1†). Molecular docking data suggested that **QMT-SFA** has a high binding energy with sulfatase (−6.19 kcal mol^{-1}). The above results demonstrated the good binding ability between **QMT-SFA** and sulfatase, which permitted efficient enzymatic interactions.

We further investigated the potential of **QMT-SFA** in imaging intracellular sulfatase activity. Before cell imaging, the cytotoxicity of **QMT-SFA** was evaluated in 4T1 cells by 3-(4,5-dimethylthiazol-2-yl)-2,5-diphenyltetrazolium bromide (MTT) assay. As shown in Fig. S5,† after incubation with **QMT-SFA** at different concentrations (up to 320 μM), 4T1 or L02 cells retained high-level viability (>80%), indicating the low cytotoxicity of **QMT-SFA**. We then tested whether **QMT-SFA** could be used for sulfatase activity imaging in 4T1 cells. Time-course fluorescence images of **QMT-SFA**-treated 4T1 cells indicated that the fluorescence of 4T1 cells rapidly increased with time and reached its maximum at 1 h (Fig. S6†), suggesting the fast activation of **QMT-SFA** in 4T1 cells. Then, we chose 1 h as the incubation time of **QMT-SFA** in the following cell experiments. As shown in Fig. 3, 4T1 cells incubated with 10 μM **QMT-SFA** showed bright AIE fluorescence, suggesting that **QMT-SFA** was activated by cellular sulfatase. In contrast, L02 (a normal cell that has undetectable sulfatase) showed negligible AIE fluorescence after incubation with 10 μM **QMT-SFA** for 1 h. Moreover, when the cells were pre-incubated with a 1 mM sulfatase inhibitor (hydroxylamine) for 0.5 h, no obvious red fluorescence was observed after **QMT-SFA** treatment, demonstrating that **QMT-SFA** was indeed activated by intracellular sulfatase. The above results indicated that **QMT-SFA** could be used for the sensitive imaging of intracellular sulfatase activity.

Inspired by its excellent performance, we further employed **QMT-SFA** to monitor sulfatase *in vivo*. The 4T1 tumor-bearing nude mice were randomly divided into two groups. Briefly, mice in one group were merely intratumorally injected with 0.25 mg kg^{-1} **QMT-SFA** (*i.e.*, the "QMT-SFA" group), while those in the other group were pre-injected with hydroxylamine for 0.5 h, followed by the injection with **QMT-SFA** (*i.e.*, the

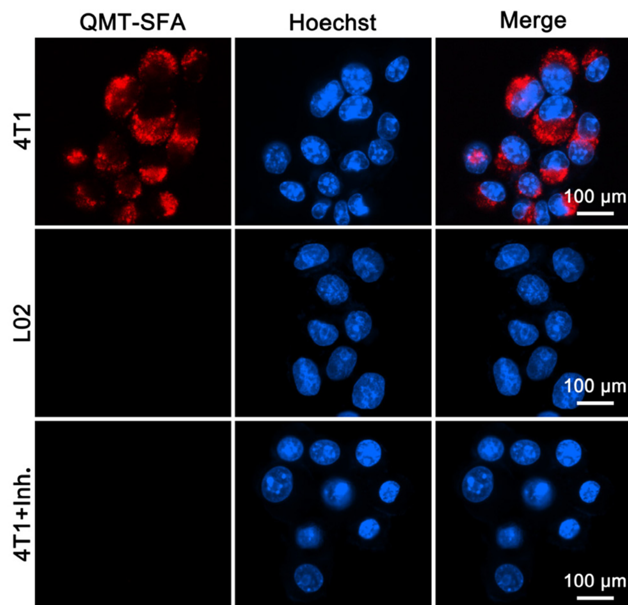

Fig. 3 Fluorescence images of 10 μM **QMT-SFA**-treated 4T1 cells, L02 cells, and hydroxylamine-pretreated 4T1 cells for 1 h.

"QMT-SFA + Inh." group). The fluorescence signals of the tumor regions were monitored by a small animal imaging system. As shown in Fig. 4, for the mice in the "QMT-SFA" group, the fluorescence within the tumor region was quickly turned "on" and reached the strongest brightness at 1 h post-injection, followed by a slow decrease within 16 h (Fig. S7†). In contrast, for the mice in the "QMT-SFA + Inh." group, a significantly low-level fluorescence profile was observed within the tumor region. The above results illustrated that **QMT-SFA** can be hydrolyzed by sulfatase to turn its NIR AIE fluorescence "on" in 4T1 tumor-bearing nude mice. In addition, the biodistribution of **QMT-SFA** in the above nude mice was further observed by *ex vivo* fluorescence imaging. As shown in Fig. S8,† fluorescence was undetectable in the major mouse organs (*i.e.*, heart, liver, spleen, lungs, and kidney) from both groups, as well as in the tumor from the "QMT-SFA + Inh." group. In contrast, the tumor from the "QMT-SFA" group showed a strong NIR fluorescence. These *in vivo* results demonstrated that **QMT-SFA** could be applied for sulfatase imaging in tumors of living animals.

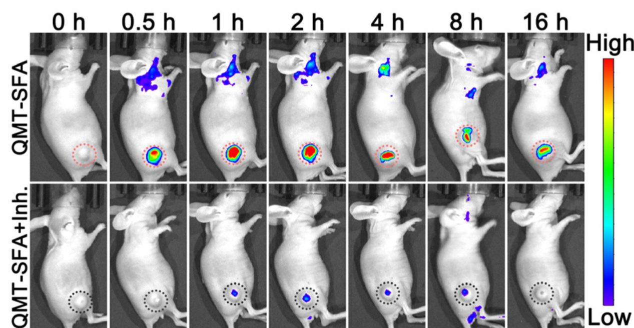

Fig. 4 Time-course fluorescence images of 4T1 tumor-bearing mice after the intratumoral injection of 0.25 mg kg^{-1} **QMT-SFA**. For the "QMT-SFA + Inh." group, tumors were pretreated with 0.02 mg kg^{-1} inhibitor for 0.5 h before **QMT-SFA** injection. The dashed circles indicate tumor regions.

Conclusions

In summary, we have successfully designed an NIR fluorescence probe **QMT-SFA** for the sensitive detection of sulfatase *in vitro* and imaging sulfatase activity in tumors of living mice. **QMT-SFA** could be cleaved by sulfatase to yield **QMT-OH**, which thereby aggregated into nanoparticles to turn the NIR AIE fluorescence "on" (centered at 660 nm). The probe exhibited high sensitivity toward sulfatase with an LOD of 0.26 U mL^{-1} *in vitro*. Molecular docking calculation showed that **QMT-SFA** had a high binding affinity (−6.19 kcal mol^{-1}) with the sulfatase docking score. In addition, **QMT-SFA** had been successfully employed for tracking sulfatase in 4T1 cells and 4T1 tumor-bearing nude mice. To the best of our knowledge, **QMT-SFA** was the first NIR AIEgen for sulfatase imaging in living cells and animals. Compared with current sulfatase AIEgens which emit visible light, **QMT-SFA** has higher potential in biological application owing to its improved tissue penetration and suppressed autofluorescence interference. We anticipate that this NIR AIEgen **QMT-SFA** could be employed for the early diagnosis of sulfatase-associated disease in clinic in near future.

Author contributions

Lingling Xu: investigation, formal analysis, methodology, validation, visualization, and writing – original draft. Yu Deng: investigation and validation. Hang Gao: validation and project administration. Yuchen Yao: validation. Xiaoyang Liu: visualization and formal analysis. Wenjun Zhan: supervision and project administration. Gaolin Liang: funding acquisition, project administration, supervision, and writing – review & editing. Xianbao Sun: conceptualization, funding acquisition, project administration, and writing – review & editing.

Ethical statement

All animal experiments were approved and performed according to the guidelines of the Animal Care and Use Committee of the Southeast University Laboratory Animal Center (No: 20240306009).

Conflicts of interest

The authors declare no conflict of interest.

Published on 30 May 2024. Downloaded on 5/21/2026 4:37:46 PM.

 This journal is © The Royal Society of Chemistry 2024

Published on 30 May 2024. Downloaded on 5/21/2026 4:37:46 PM.

Acknowledgements

This work was supported by the National Natural Science Foundation of China (Grants 22204019 and 22234002), the Full-time Talents Program of Hebei Province (Grant 2023HBQZYCXY027), and the China Postdoctoral Science Foundation funded project (Grant 2023M730577).

References

1 S. Loibl, P. Poortmans, M. Morrow, C. Denkert and G. Curigliano, *Lancet*, 2021, **397**, 1750–1769.
2 A. N. Giaquinto, H. Sung, K. D. Miller, J. L. Kramer, L. A. Newman, A. Minihan, A. Jemal and R. L. Siegel, *CA Cancer J. Clin.*, 2022, **72**, 524–541.
3 D. Barba, A. León-Sosa, P. Lugo, D. Suquillo, F. Torres, F. Surre, L. Trojman and A. Caicedo, *Crit. Rev. Oncol. Hematol.*, 2021, **157**, 103174.
4 I. H. Kunkler, L. J. Williams, W. J. L. Jack, D. A. Cameron and J. M. Dixon, *N. Engl. J. Med.*, 2023, **388**, 585–594.
5 D. Yue, M. Wang, F. Deng, W. Yin, H. Zhao, X. Zhao and Z. Xu, *Chin. Chem. Lett.*, 2018, **29**, 648–656.
6 S. R. Hanson, M. D. Best and C.-H. Wong, *Angew. Chem., Int. Ed.*, 2004, **43**, 5736–5763.
7 R. Mashima and M. Nakanishi, *Int. J. Mol. Sci.*, 2022, **23**, 8153.
8 L. Xu, N. Liu, W. Zhan, Y. Deng, Z. Chen, X. Liu, G. Gao, Q. Chen, Z. Liu and G. Liang, *ACS Nano*, 2022, **16**, 19328–19334.
9 X. Wu, R. Wang, N. Kwon, H. Ma and J. Yoon, *Chem. Soc. Rev.*, 2022, **51**, 450–463.
10 S. He, P. Cheng and K. Pu, *Nat. Biomed. Eng.*, 2023, **7**, 281–297.
11 J. Li, H. Gao, R. Liu, C. Chen, S. Zeng, Q. Liu and D. Ding, *Sci. China: Chem.*, 2020, **63**, 1428–1434.
12 M. H. Xiang, Z. Y. Jiang, W. L. Zhao, E. Zhang, L. Xia, R. M. Kong, Y. Zhao, W. Kong, X. Liu, F. Qu and W. Tan, *ACS Sens.*, 2023, **8**, 2021–2029.
13 L. Xu, H. Gao, W. Zhan, Y. Deng, X. Liu, Q. Jiang, X. Sun, J.-J. Xu and G. Liang, *J. Am. Chem. Soc.*, 2023, **145**, 27748–27756.
14 Z. Zhu, Q. Wang, X. Chen, Q. Wang, C. Yan, X. Zhao, W. Zhao and W. H. Zhu, *Adv. Mater.*, 2022, **34**, e2107444.
15 S. Jia, Z. Gao, Z. Wu, H. Gao, H. Wang, H. Ou and D. Ding, *CCS Chem.*, 2022, **4**, 501–514.
16 J. Qi, H. Ou, Q. Liu and D. Ding, *Aggregate*, 2021, **2**, 95–113.
17 Y. Xu, M. Cui, W. Zhang, T. Liu, X. Ren, Y. Gu, C. Ran, J. Yang and P. Wang, *Chem. Eng. J.*, 2022, **428**, 132514.
18 L. Xu, H. Gao, Y. Deng, X. Liu, W. Zhan, X. Sun, J. J. Xu and G. Liang, *Biosens. Bioelectron.*, 2024, **255**, 116207.
19 H. Shen, F. Sun, X. Zhu, J. Zhang, X. Ou, J. Zhang, C. Xu, H. H. Y. Sung, I. D. Williams, S. Chen, R. T. K. Kwok, J. W. Y. Lam, J. Sun, F. Zhang and B. Z. Tang, *J. Am. Chem. Soc.*, 2022, **144**, 15391–15402.